ChemComm

COMMUNICATION

View Article Online
View Journal | View Issue



Cite this: *Chem. Commun.*, 2026, **62**, 7198

Received 21st November 2025,
Accepted 13th March 2026

DOI: 10.1039/d5cc06632h

rsc.li/chemcomm

# Enhancing catalytic amine regeneration in $CO_2$ capture using $ZrO_xH_y$-coated mesoporous silica

Cheng Zhou, *[a] Yuewen Shao,[a] Mostafa Torka Beydokhti,[a] Jing Ma,[a] Pierre Eloy,[b] Damien P. Debecker,[b] Michiel Dusselier,[a] Walter Vermeiren[c] and Bert F. Sels *[a]

**Bulk $ZrO_xH_y$ is an effective catalyst for amine regeneration in $CO_2$ absorption, but its high cost and poor support stability may hinder application. Here, $ZrO_xH_y$ is deposited as a theoratical monolayer within MCM-41 mesopores, achieving similar stable catalytic activity to bulk $ZrO_xH_y$ with just 13 wt% Zr loading, offering a cost-effective path toward industrial use.**

Post-combustion $CO_2$ capture using aqueous amine solvents is widely regarded as the most practical short-term strategy for large-scale mitigation of greenhouse gas emissions from existing power plants and industrial facilities.[1,2] Despite its maturity, conventional thermal regeneration of amine solutions remains highly energy-intensive.[3] This is mainly due to the slow kinetics of $CO_2$ desorption at moderate temperatures, while amine degradation at elevated temperatures further increases operating costs.[4–6] To address this bottleneck, catalytic amine regeneration has emerged as an approach, offering the potential to accelerate desorption kinetics while reducing the energy consumption.[7–14]

Among the catalysts reported to date, zirconium oxo-hydroxide ($ZrO_xH_y$) materials have demonstrated very recently outstanding activity for promoting amine regeneration, with excellent performance confirmed under both batch and continuous reactor configurations.[15,16] Despite their promise, the direct application of bulk $ZrO_xH_y$ in industrial settings is hindered by the need for supported catalysts with stronger mechanical strength and the relatively high cost of zirconium compared to silicon.[17,18] To date, achieving a uniform and accessible dispersion of $ZrO_xH_y$ on a support, without compromising catalytic performance, has remained uncertain.

In this work, we demonstrate a cost-effective strategy to harness the exceptional catalytic properties of $ZrO_xH_y$ through its controlled deposition within the mesoporous framework of MCM-41 (Zr-MCM-41). Remarkably, with only 13 wt% zirconium loading, the resulting supported catalyst delivers activity comparable to bulk $ZrO_xH_y$ per total catalyst mass. This high efficiency is attributed to the uniform high dispersion of active $ZrO_xH_y$ species on the mesopore walls, maintaining full accessibility of the porous network. Importantly, no detrimental interaction between MCM-41 and $ZrO_xH_y$ was detected, highlighting the structural and mechanistic fidelity of the active phase and its promise for scalable amine regeneration catalysis.

The original bulk $ZrO_xH_y$ catalyst was synthesized *via* a sol–gel method,[15] during which the wet gel underwent more than a 80% volume reduction upon drying. Photographs depicting the shrinkage of the $ZrO_xH_y$ gel before and after drying are shown in Fig. S1. This substantial contraction facilitates the deposition of the material within a porous $SiO_2$ support without blocking its inherent pore network. While MCM-41 is a commercialized $SiO_2$ support with ordered straight meso-pores. MCM-41, a well-established commercial mesoporous silica featuring a highly ordered channel structure, was chosen as the support material.

As illustrated in Fig. 1a, MCM-41 powder was mixed with a $ZrO(NO_3)_2$ precursor solution. The abundant surface Si–OH groups of MCM-41 provide anchoring sites for the Zr hydrogel at the gel–support interface. During drying at 100 °C, condensation of the wet gel induces significant volume contraction. Within the 2.5 nm mesopores, however, spatial confinement and capillary forces, together with strong interfacial Si–O(H)–Zr bonding, stabilize the gel–wall interface and prevent detachment or particle segregation. As a result, shrinkage occurs primarily along the pore walls, producing a uniform, conformal $ZrO_xH_y$ coating. This is proved in Fig. 1b, $N_2$ adsorption–desorption isotherms of pristine and $ZrO_xH_y$-coated MCM-41 retain the characteristic Type-IV profile, indicating that mesoporosity and pore ordering are largely preserved. The coated sample shows reduced adsorption volume and surface area (Table S1), reflecting partial thickening of the pore walls by $ZrO_xH_y$. Additionally, the coated sample displays a reduced high-pressure uptake, suggesting a decrease in interparticle

[a] *Center for Sustainable Catalysis and Engineering, KU Leuven, Celestijnenlaan 200F, Heverlee 3001, Belgium. E-mail: cheng.zhou@kuleuven.be, bert.sels@kuleuven.be*
[b] *Université catholique de Louvain (UCLouvain), Institute of Condensed Matter and Nanosciences (IMCN), Place Louis Pasteur, 1, Louvain-la-Neuve 1348, Belgium*
[c] *TotalEnergies OneTech Belgium, Zone industrielle C, Feluy 7181, Belgium*

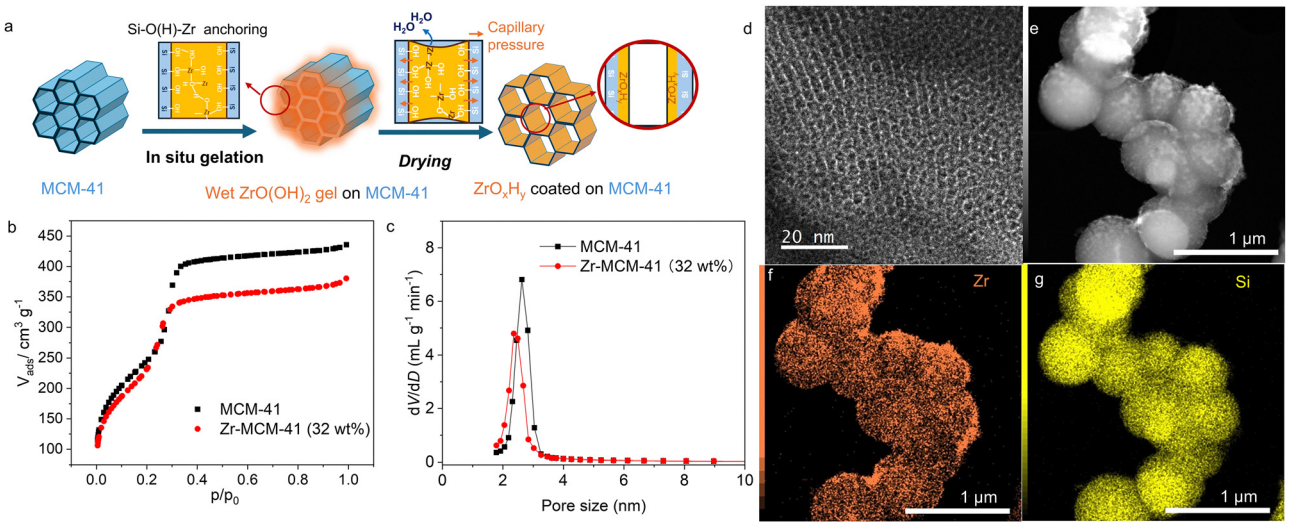


Fig. 1 (a) Schemes of coating $ZrO_xH_y$ on MCM-41. (b). $N_2$ physisorption isotherms and (c) pore size distribution of MCM-41 and Zr-MCM-41 (32 wt%). (d) HR-TEM and (e) TEM image of Zr-MCM-41 (32 wt%). (f) and (g) EDX mapping TEM of Zr-MCM-41 (32 wt%) with element of Zr and Si.

voids and implying the presence of $ZrO_xH_y$ on the external particle surfaces. Pore size distributions (Fig. 1c) show a narrow peak at 2.8 nm for MCM-41, which shifts slightly to 2.5 nm after $ZrO_xH_y$ coating. The ~0.3 nm wall thickness increase is consistent with the theoretical monolayer thickness of $ZrO_xH_y$, suggesting a near-monolayer coverage. The mesopore volume decreases from 0.77 to 0.54 $cm^3\ g^{-1}$, corresponding to ~28 wt% Zr (assuming all volume loss is due to $ZrO_xH_y$ with a density of 3.25 $g\ cm^{-3}$), in close agreement with ICP measurements (32 wt%), confirming that most $ZrO_xH_y$ resides within the mesoporous channels.

Transmission electron microscopy (TEM) images of Zr-MCM-41(32 wt%) (Fig. 1d and Fig. S2) reveal well-defined mesoporous channels without distinct $ZrO_xH_y$ particles, indicating a uniform, conformal in-pore coating. Energy Dispersive X-ray Spectroscopy (EDX-TEM) (Fig. 1f and g) confirms homogeneous Zr distribution throughout the MCM-41 particles except for the external surface, where an oligomerized from $ZrO_xH_y$ particles and thicker $ZrO_xH_y$ layer are witness (Fig. S3), and reflecting unrestricted gel growth outside the spatially confined mesopores. The high Zr content on the external surface is further quantified by X-ray photoelectron spectroscopy (XPS), which gives a Zr/Si ratio of 0.29, corresponding to ~43 wt% Zr, which is higher than the bulk value. However, considering the small external surface area of MCM-41, this external Zr accounts for only ~4.8% of the total Zr, meaning that over 95% of Zr remains well confined within the mesoporous channels without blocking the pores.

The catalytic activity of Zr-MCM-41 (32 wt%) for $CO_2$ desorption was evaluated in a batch reactor (Fig. S4) using 30 wt% $CO_2$-rich monoethanolamine (MEA), the standard industrial solvent. The mixture was heated from 25 °C to 88 °C and held isothermally for 3 hours. For comparison, desorption was also tested with bulk $ZrO_xH_y$, pristine MCM-41, and without any catalyst (blank).

Fig. 2a shows the $CO_2$ loading ($mol_{CO2}\ mol_{amine}^{-1}$) over time. Bulk $ZrO_xH_y$ markedly accelerates desorption during both heating and isothermal stages, while MCM-41 shows negligible effect. Zr-MCM-41 (32 wt%) achieves nearly the same enhancement as bulk $ZrO_xH_y$. The isothermal catalytic rate constant ($k_{CAT}$), calculated assuming first-order kinetics[19] after subtracting the thermal background (Fig. 2b), is $2.9 \times 10^{-4}$ $min^{-1}$ for

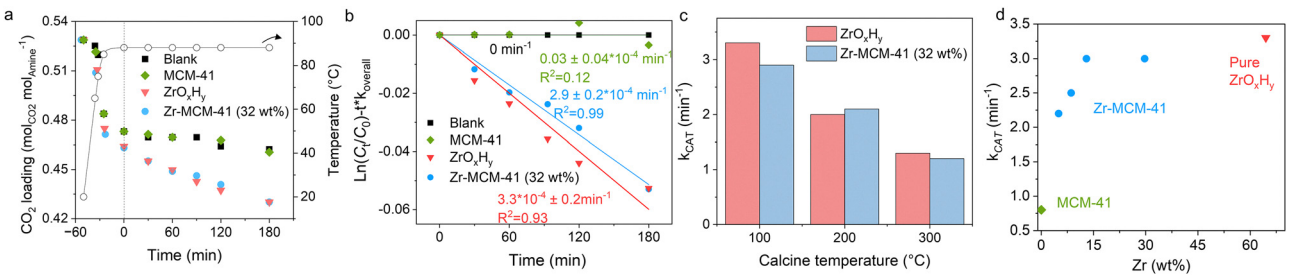


Fig. 2 (a) $CO_2$ desorption performance and (b) kinetic analysis during the isothermal stage, with the *y*-axis representing the catalytic contribution calculated from the overall reaction rate constant after subtracting the thermal background. Time zero corresponds to the start of the isothermal stage at 88 °C. (c) Effect of calcination temperature on $k_{CAT}$ for bulk $ZrO_xH_y$ and Zr-MCM-41 (32 wt%). (d) Relationship between the catalytic rate constant ($k_{CAT}$) and Zr loading (Zr wt% of total solid). Reaction conditions: 150 mL $CO_2$-saturated 30 wt% MEA, 3 g catalyst, $N_2$ flow 0.5 L $min^{-1}$ at the condenser top, 88 °C.

Zr-MCM-41, comparable to bulk $ZrO_xH_y$ ($3.3 \times 10^{-4}$ $min^{-1}$). MCM-41 itself exhibits a minimal $k_{CAT}$ of $0.02 \times 10^{-4}$ $min^{-1}$, confirming that the activity originates exclusively from the $ZrO_xH_y$ coating. The overall kinetic (with thermal background) is shown in the Fig. S5, with good linearity.

$ZrO_xH_y$ is known to be sensitive to thermal treatment, as dehydration reduces the surface hydroxyl groups responsible for its catalytic activity. In this study, Zr-MCM-41 (32 wt%) exhibited a similar trend of activity loss with increasing calcination temperature as bulk $ZrO_xH_y$ (Fig. 2c), though the decline was noticeably less pronounced. After calcination at 200 °C, Zr-MCM-41(32 wt%) retained 72% of its initial activity, compared to 60% for bulk $ZrO_xH_y$; at 300 °C, the retained activity was 41% *versus* 39%, respectively. These results indicate that while some loss of active surface hydroxyls during calcination is unavoidable, supporting $ZrO_xH_y$ on mesoporous silica such as MCM-41 can substantially mitigate deactivation, preserving a greater fraction of the catalytic performance.

Zr with different loading was carried out, as shown in Fig. 2d, although increasing Zr loading initially enhances the desorption rate, further increases beyond 13 wt% do not result in proportional $k_{CAT}$ enhancement. The Weisz–Prater criterion was applied to Zr-MCM-41 (32 wt%), yielding $C_{WP} \ll 1$ (see SI for detailed calculations), ruling out intraparticle diffusion limitations. The observed rate plateau therefore likely reflects reduced Zr utilization at higher loadings, suggesting that more dispersed Zr may be preferred. Since $ZrO_xH_y$ was mostly coated on the pore wall for 32 wt% loading, the decrease on the activity should not relate to aggregation of the Zr. TEM images (Fig. S6) reveal well-defined mesoporous channels without discernible $ZrO_xH_y$ nanoparticles, indicating the absence of segregated oxide domains. EDX mapping of Zr-MCM-41 (13 wt%) (Fig. S7) shows a dilute yet homogeneous Zr distribution that closely follows the silica framework, in contrast to the higher local intensity observed at 32 wt% loading. As calculated in previous, a full monolayer $ZrO_xH_y$ coating on MCM-41 theoretically requires at least 28 wt% Zr, suggesting that at lower loadings a significant fraction of the $SiO_2$ surface remains exposed. It is further supported by additional experiments using conventional amorphous $SiO_2$ with lower surface area (254 $m^2$ $g^{-1}$), where Zr–$SiO_2$ exhibits a much lower $k_{CAT}$ of $2.3 \times 10^{-4}$ $min^{-1}$, at similar Zr loading (13 wt%).

To further clarify the nature of the active sites in the supported catalysts, *in situ* diffuse reflectance infrared Fourier transform spectrometry (DRIFTS) measurements were performed on MCM-41 and Zr-MCM-41 samples with Zr loadings of 13 wt% and 32 wt% at different temperatures under $N_2$ (Fig. 3a–c). The sharp band at ~3740 $cm^{-1}$, attributed to isolated Si–OH groups, progressively decreases with increasing Zr loading, while a new band near ~3550 $cm^{-1}$ and a broad feature centered around ~3400 $cm^{-1}$ emerge and intensify. These lower-frequency and broader bands indicate the formation of Zr-related hydroxyl

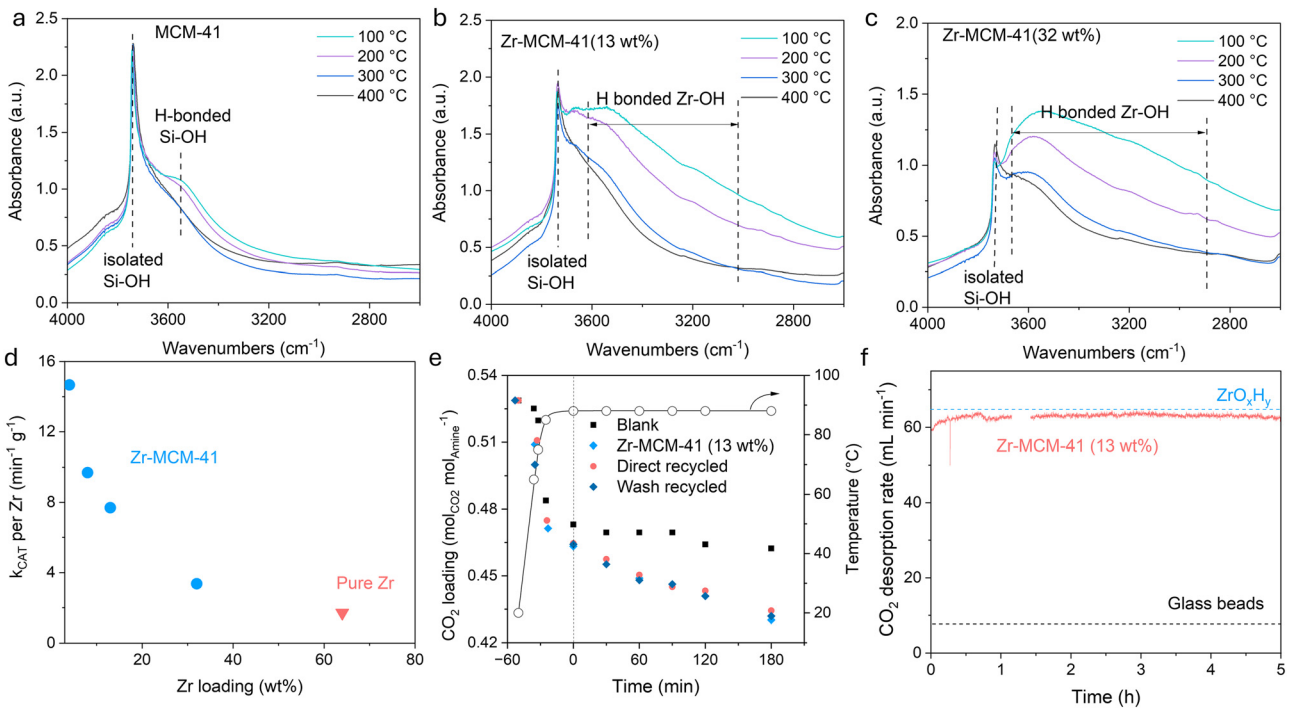


Fig. 3 *In situ* DRIFS under different temperature (a) MCM-41, (b) Zr-MCM-41 (13 wt%) (c) Zr-MCM-41 (32 wt%). (d) Zr mass normalized $k_{CAT}$ ($min^{-1}$ $g^{-1}$) *versus* Zr loading amount. (e) Zr-MCM-41 (13 wt%) catalyst regeneration performance. Reaction conditions: 150 mL $CO_2$-saturated 30 wt% MEA, 3 g catalyst, $N_2$ flow of 0.5 L $min^{-1}$ from the top of the condenser, 88 °C. (f) $CO_2$ desorption rate from 30 wt% MEA for a 16 ± 2% regeneration ratio in the continuous reactor set-up with shaped Zr-MCM-41 (13 wt%). Reaction condition: 88 °C, $CO_2$ partial pressure of 25 ± 5 kPa as determined by MS, 6 g catalyst, particle diameter of 0.25 to 0.5 mm. The glass beads with similar sizes of catalyst are used in the blank to exclude the influence of bed porosity. The $CO_2$ desorption rate of $ZrO_xH_y$ and glass beads data was taken from reported data under same condition.[15]

 

species with stronger hydrogen-bonding interactions, which are absent in pristine MCM-41. Notably, no new hydroxyl species are observed when comparing the 13 wt% and 32 wt% Zr-loaded samples; the primary difference lies in the relative abundance of Zr-OH and Si-OH groups rather than their nature.

When normalized by Zr loading mass, as shown in Fig. 3d, the Zr-specific activity decreases roughly logarithmically with increasing Zr content. This trend suggests that higher surface density reduces the effective turnover per Zr site, which can be up to 8.6 times higher than that of pure $ZrO_xH_y$. Additionally, the support effect may also impact the activity of individual Zr sites, specifically the influence of exposed Si–OH groups on Zr, as reported in previous studies,[20] though further investigation is needed to fully clarify this effect.

Catalyst recyclability is a key factor in evaluating performance. For Zr-MCM-41 (13 wt%), the catalyst can be regenerated through both water-wash recycling and direct reuse (detailed in Fig. S8) without significant loss of activity (Fig. 3e).

The catalyst was evaluated in a continuous fixed-bed reactor for 5 h without noticeable deactivation, exhibiting performance comparable to that of pure $ZrO_xH_y$ (Fig. 3f). During this period, the activity of Zr-MCM-41 (13 wt%) remained essentially constant, indicating stable intrinsic active sites under the applied desorption conditions. Prolonged operation, however, led to deterioration of the packed bed, as the shaped catalyst bodies disintegrated into fine particles and were washed out by the liquid flow. This behavior indicates that the observed stability limitation arises primarily from insufficient mechanical strength and bed integrity under high gas–liquid flux, rather than from chemical deactivation of the $ZrO_xH_y$ active phase. Future work should therefore focus on improving catalyst shaping and mechanical robustness for long-term operation.

This study demonstrates the successful development of a high-performance $ZrO_xH_y$ catalyst uniformly coated onto the mesopore walls of MCM-41. The resulting Zr-MCM-41 combines exceptional catalytic activity, comparable to bulk $ZrO_xH_y$, with a remarkably low Zr loading of just 13 wt%. While calcination inevitably reduces activity, the supported catalyst exhibits less deactivation than the unsupported counterpart, highlighting the stabilizing effect of the mesoporous support. Together, these results provide compelling evidence that Zr-MCM-41 is a cost-efficient, robust, and scalable catalyst, offering significant promise for practical implementation in industrial $CO_2$ amine-regeneration processes. Future works may focusing on high mechanical strengthen shaped catalyst and investigation of lower-cost, high-surface-area commercial supports, such as activated carbon.

## Conflicts of interest

There are no conflicts to declare.

## Data availability

The data supporting this article have been included in the main text and supplementary information (SI). Supplementary information is available. See DOI: https://doi.org/10.1039/d5cc06632h.

## Acknowledgements

C. Z. acknowledge Walter Vermandel for technical supports. B. F. S. acknowledges TotalEnergies for financial support. M. T. B. and M. D. thank the European Research Council (ERC) for funding: ERC Starting Grant 948449 named Z-EURECA, *i.e.*, Zeolite synthesis in Unusual Reactors for Enhanced Catalysts to MD. The TEM-EDS in this research was supported by the FWO infrastructure projects (AKUL13/19 and I000920N). The $N_2$ physisorption research was supported by KUL internal funding, KA/16/064. The DRIFTS was supported by FWO, G0A0321N.

## References

1 S. Chu, *Science*, 2009, **325**, 1599.
2 IEA, Energy Technology Perspectives 2020, https://www.iea.org/reports/energy-technology-perspectives-2020.
3 C. Zou, Q. Zhao, G. Zhang and B. Xiong, *Nat. Gas Ind. B*, 2016, **3**, 1–11.
4 F. Raganati and P. Ammendola, *Energy Fuels*, 2024, **38**, 13858–13905.
5 F. de Meyer and C. Bignaud, *Chem. Eng. J.*, 2022, **428**, 131264.
6 S. Nakao, K. Yogo, K. Goto, T. Kai and H. Yamada, *Advanced CO2 capture technologies: Absorption, adsorption, and membrane separation methods*, 2019.
7 X. Li, L. Xing, Z. Chen, Y. Wang, C. Wang, G. Zhan, H. Chang and J. Li, *Adv. Funct. Mater.*, 2025, **2414293**, 1–10.
8 X. Zhong, W. Kong, K. Yang, T. Song, Z. Dong, L. Liang, S. Zhang, W. Li and S. Li, *Adv. Funct. Mater.*, 2025, **2422336**, 1–16.
9 Y. Li, L. Xing, Z. Chen, G. Zhan, B. Yuan, Y. Peng, L. Wang and J. Li, *Appl. Catal., B*, 2024, **358**, 124350.
10 Q. Sun, H. Gao, M. Xiao, T. Sema and Z. Liang, *Environ. Sci. Technol.*, 2024, **58**, 10052–10059.
11 C. Zhou, J. Shi, W. Zhou, K. Cheng, Q. Zhang, J. Kang and Y. Wang, *ACS Catal.*, 2019, **10**, 302–310.
12 C. Zhou, I. Khalil, F. Rammal, M. Dusselier, P. Kumar, M. Lacroix, E. Makshina, Y. Liao and B. F. Sels, *ACS Catal.*, 2022, **12**, 11485–11493.
13 M. S. Alivand, O. Mazaheri, Y. Wu, A. Zavabeti, A. J. Christofferson, N. Meftahi, S. P. Russo, G. W. Stevens, C. A. Scholes and K. A. Mumford, *Nat. Commun.*, 2022, **13**, 1–11.
14 Q. Lai, S. Toan, M. A. Assiri, H. Cheng, A. G. Russell, H. Adidharma, M. Radosz and M. Fan, *Nat. Commun.*, 2018, **9**, 1–7.
15 C. Zhou, M. T. Beydokhti, F. Rammal, P. Kumar, M. Lacroix, W. Vermeiren, M. Dusselier, Y. Liao and B. F. Sels, *Nat. Catal.*, 2025, **8**, 270–281.
16 L. Ji, J. Li, R. Zhai, J. Wang, X. Wang, S. Yan and M. Hua, *ACS Omega*, 2022, **7**, 44620–44630.
17 R. J. Farrauto, *Handbook of Industrial Chemistry and Biotechnology*, 2017, pp. 1995–2035.
18 D. Leybo, U. J. Etim, M. Monai, S. R. Bare, Z. Zhong and C. Vogt, *Chem. Soc. Rev.*, 2024, **53**, 10450–10490.
19 P. V. Danckwerts, *Chem. Eng. Sci.*, 1979, **34**, 443–446.
20 X. Zhang, Y. Huang, J. Yang, H. Gao, Y. Huang, X. Luo, Z. Liang and P. Tontiwachwuthikul, *Chem. Eng. J.*, 2020, **383**, 123077.